JOC Article

N-tert-Butoxy-1-aminopyrenyl Radicals. Isolation, Electronic Structure, and Magnetic Characterization[1]

Yozo Miura,* Nobuaki Matsuba, and Rika Tanaka

Department of Applied Chemistry, Graduate School of Engineering, Osaka City University, Sumiyoshi-ku, Osaka 558-8585, Japan

Yoshio Teki and Takeji Takui

Department of Material Science and Chemistry, Graduate School of Science, Osaka City University, Sumiyoshi-ku, Osaka 558-8585, Japan

miura@a-chem.eng.osaka-cu.ac.jp

Received April 18, 2002

N-tert-Butoxy-2,7-di-*tert*-butyl-1-pyrenylaminyl (**4**), *N-tert*-butoxy-2-*tert*-butyl-1-pyrenylaminyl (**5**), and *N-tert*-butoxy-7-*tert*-butyl-1-pyrenylaminyl (**6**) free radicals were generated by the reaction of the lithium amides of the corresponding 1-aminopyrenes with *tert*-butyl peroxybenzoate in THF at −78 °C. Although **6** could not be isolated due to the gradual decomposition in solution, **4** and **5** were quite persistent and could be isolated as monomeric radical crystals. The X-ray crystallographic analyses for the isolated free radicals were successfully carried out, indicating that the N and O atoms are almost coplanar with the pyrene ring. The ESR spectra of **4** and **5** were very complex due to the presence of many magnetically unequivalent protons. Therefore, the proton hyperfine coupling (hfc) constants were determined by ^{1}H ENDOR/TRIPLE resonance spectroscopy. To assign the hfc constants for the pyrene ring protons, a partially deuterated radical, **4**-d_4, was prepared and the ENDOR and ESR spectra were measured. To discuss the spin density distribution for **4** and **5** ab initio molecular orbital calculations were performed by the DFT UBecke 3LYP method, using the STO 6-31G basis set. Magnetic susceptibility measurements were carried out for **4** and **5** with a SQUID magnetometer. For **4** a weak antiferromagnetic interaction was observed, and for **5** a very strong antiferromagnetic interaction was observed. The antiferromagnetic interactions were explained by their crystal structures.

Introduction

Although a variety of oxyaminyls have been widely studied over a long period,[2] the first isolation of oxyaminyl radicals (RṄOR′) by our group was quite recent.[1,3] This is in contrast to the chemistry of isoelectronic thioaminyls (RṄSR′).[4] A variety of thioaminyl radicals can be readily prepared by oxidation of sulfenamides (RNHSR′), which can be obtained by the reaction of amines with sulfenyl halides,[5] with PbO_2. This easy preparation of thioaminyls has allowed extensive studies on thioaminyls in recent years.[4] For alkoxyaminyls, on the other hand, an easy and a widely applicable procedure for their preparation has not been reported yet. Quite recently, we found three kinds of stable oxyaminyls, **1**−**3** (Chart 1), can be prepared by the reaction of lithium amides of the corresponding anilines with *tert*-butyl peroxybenzoate.[1,3,7] Interestingly, these radicals were oxygen insensitive and could be isolated as monomeric radical crystals. Oxygen insensitive and isolable stable free radicals have attracted much attention as a building block or magnetic spin source in the construction of organic magnetic materials.[6] In the extension of this study, we have searched for other isolable oxyaminyl radicals. Although we prepared anthracene ring-bearing and pyrene ring-bearing oxyaminyls, only the pyrene ring-bearing oxyaminyl radicals, **4** and **5** (Chart 1), can

* To whom correspondence should be address. Phone: +81-6-6605-2798. Fax: +81-6-6605-2769

(1) ESR Studies of Nitrogen-Centered Free Radicals. 55. For part 54, see: Miura, Y.; Tomimura, T.; Matsuba, N.; Tanaka, R.; Nakatsuji, M. *J. Org. Chem*. **2001**, *66*, 7456−7463.

(2) Danen, W. C.; Neugebauer, F. A. *Angew. Chem., Int. Ed. Engl.* **1975**, *14*, 783. Danen, W. C.; West, C. T.; Kensler, T. T. *J. Am. Chem. Soc*. **1973**, *95*, 5716. Kaba, R. A.; Ingold, K. U. *J. Am. Chem. Soc*. **1976**, *98*, 7375. Woynar, H.; Ingold, K. U. *J. Am. Chem. Soc*. **1980**, *102*, 3813. Ahrens W.; Wieser, K.; Berndt, A. *Tetrahedron Lett*. **1973**, 3141. Balaban, A. T.; Frangopol, P. T.; Frangopol, M.; Negoitå, N. *Tetrahedron* **1967**, *23*, 4661. Terabe, S.; Konaka, R. *J. Chem. Soc., Perkin Trans. 2* 1973, 369. Negoitå, N.; Baican, R.; Balaban, A. T. *Tetrahedron Lett*. 1973, 1877. Ahrens, W.; Berndt, A. *Tetrahedron Lett*. **1973**, 4281. Negareche, M.; Boyer, M.; Tordo, P. *Tetrahedron Lett*. **1981**, *22*, 2879.

(3) Miura, Y.; Tomimura, T. *Chem. Commun*. **2001**, 627−628.

(4) Miura, Y. *Trends Org. Chem*. **1997**, *6*, 197−217. Miura, Y. *Rec. Res. Dev. Org. Chem*. **1998**, *2*, 251−268.

(5) For example, see: Miura, Y.; Tomimura, T.; Teki, Y. *J. Org. Chem*. **2000**, *65*, 7889−7895. Nakatsuji, M.; Miura, Y.; Teki, Y. *J. Chem. Soc., Perkin Trans. 2* **2001**, 738.

(6) *Magnetic Properties of Organic Materials*; Lahti, P. M., Ed.; Marcel Dekker: New York and Basel, 1999. *Molecular Magnetism*; Itoh, K., Kinoshita, M., Eds.; Kodansha/Gordon and Breach: Tokyo/Australia and France, 2000. Proceedings of the 7th International Conference on Molecule-Based Magnets. In *Polyhedron* **2001**, *20*, 1115−1778.

(7) Meesters, A. C. M.; Benn, M. H. *Synthesis* **1978**, 679.

10.1021/jo0202785 CCC: $22.00
Published on Web 11/09/2002

CHART 1

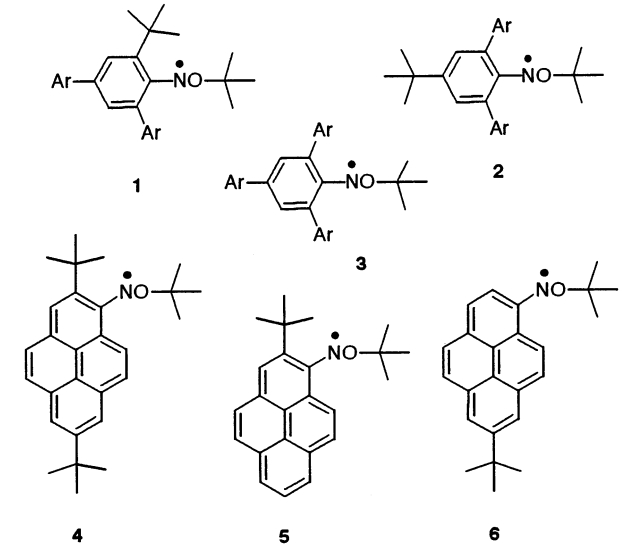

SCHEME 1

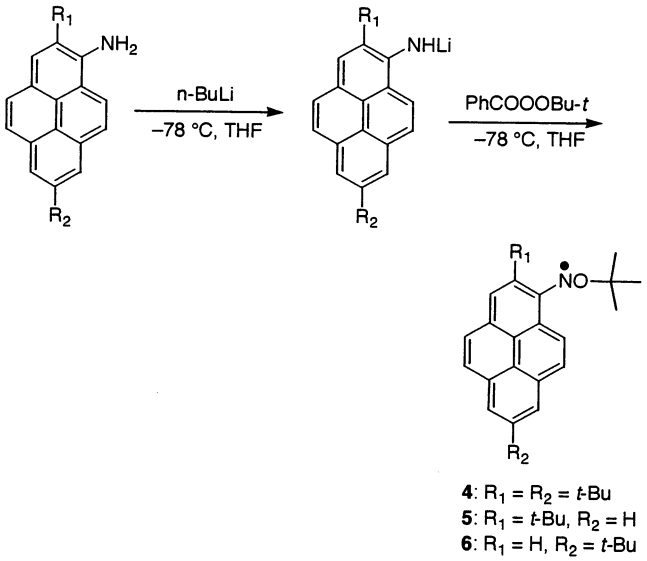

be isolated as radical crystals.[8–10] Herein we wish to report the isolation, X-ray crystallographic analyses, ESR and ^{1}H ENDOR/TRIPLE resonance spectra, and magnetic properties of **4** and **5**.

Results and Discussion

Isolation of 4 and 5. According to Scheme 1, the pyrene ring-bearing *N-tert*-butoxyaminyl radicals, **4**, **5**, and **6**, were generated by the reaction of lithium amides of the corresponding 1-aminopyrenes with 3.3 equiv of *tert*-butyl peroxybenzoate in THF at −78 °C. The procedure for the preparation of **4**−**6** is essentially the same as the previous one used for the preparation of **1**−**3**.[1] When *tert*-butyl peroxybenzoate was added to a lithium amide solution of the corresponding 1-aminopyrenes in THF at −78 °C, the originally colorless solutions immediately turned dark brown (**4** and **6**) or dark yellow (**5**), and the colors were kept for a long period. Isolation of radicals from the reaction mixtures was performed by column chromatography and subsequent recrystallization. Although **6** was decomposed during the workup and subsequent column chromatography, radicals **4** and **5** were quite long-lived under atmospheric conditions and could be successfully isolated as dark red plates (**4**) or dark green plates (**5**) in 23−27% yields. The radical structures were confirmed by the IR spectra and elemental analyses. In the IR spectra no νNH absorption was observed, and the elemental analyses gave satisfactory agreements with the calculations. The structures were later unequivocally confirmed by the X-ray crystallographic analyses, as described below.

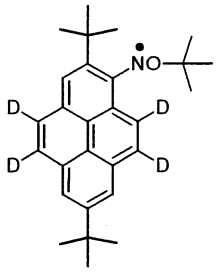

4-d_4

Thermal Stability. In a previous paper,[1] we reported that **1**−**3** were thermally very stable. This was clearly shown by the following experiment: benzene solutions of radicals in degassed Pyrex tubes were heated at 80 °C for 10 days, and the radical concentrations of the resulting solutions were measured by ESR or UV−visible spectroscopy. Surprisingly, even after heating at 80 °C for 10 days, 80% of the radicals were found to survive without decomposition. The thermal stability of **4** and **5** was evaluated by the same procedure as above. Namely, the degassed benzene solutions of **4** and **5** were heated at the same temperature for 10 days, and the resultant radical concentrations were measured by ESR using 1,3,5-triphenylverdazyl as the reference. The ESR measurements showed that, even after heating for 10 days, ∼80% of the radicals survived without decomposition, revealing that **4** and **5** have comparable thermal stability to **1**−**3**.

X-ray Crystallographic Analyses. Since, upon recrystallization from MeOH (**4**) or MeOH-EtOAc (**5**), **4** and **5** provided single crystals suitable for X-ray crystallographic analysis, X-ray crystallographic studies were performed. ORTEP drawings are shown in Figures 1 and 2, together with selected bond lengths, bond angles, and torsion angles.

Figure 1 shows that radical **4** adopts an almost planar conformation. This is clearly shown by the torsion angles for C2−C1−N1−O1 [173.0(2)°] and C14−C1−N1−O1 [-6.6(3)°]. Therefore, the N and O atoms are in the same plane with the pyrene ring. A more planar structure was shown by **5**. The torsion angles for C2−C1−N1−O1 and C14−C1−N1−O1 are −176.4(1) and −0.6(2)°, indicating an almost completely planar structure. Such planar conformations of **4** and **5** suggest that the presence of

(8) Miura, Y.; Yamano, E.; Tanaka, A.; Yamauchi, J. *J. Org. Chem.* **1994**, *59*, 3294−3300.
(9) Miura, Y.; Oka, H.; Yamano, E.; Teki, Y.; Takui, T.; Itoh, K. *Bull. Chem. Soc. Jpn.* **1995**, *68*, 1187−1192.
(10) Miura, Y.; Yamano. E. *J. Org. Chem.* **1995**, *60*, 1070−1073.

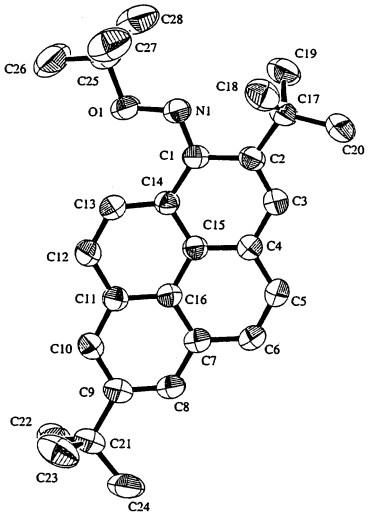

FIGURE 1. ORTEP drawing of **4**. Selected bond lengths (Å) and angles (deg) and torsion angles (deg) are as follows: N1−O1 1.379(3), C1−N1−O1 114.0(2), N1−O1−C25 111.4(2), C2−C1−N1−O1 173.0(2), C14−C1−N1−O1 −6.6(3), C1−N1−01−C25 174.4(2).

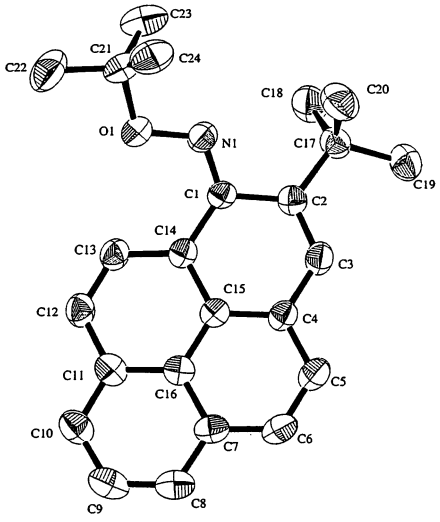

FIGURE 2. ORTEP drawing of **5**. Selected bond lengths (Å), bond angles (deg), and torsion angles (deg) are as follows: N1−O1 1.393(2), C1−N1−O1 114.2(1), N1−O1−C21 110.3(1), C2−C1−N1−O1 −176.4(1), C14−C1−N1−O1 −0.6(2), C1−N1−O1−C21 169.9(1).

the 2-*tert*-butyl group does not prevent the radicals from adopting a planar structure.

ESR, ^{1}H ENDOR, and ^{1}H TRIPLE Resonance Spectroscopy. The ESR spectra of **4** and **5** were recorded at room temperature (23 °C), using benzene as the solvent. A typical ESR spectrum of **4** is depicted in Figure 3. As had been expected, the ESR spectra for **4** and **5** were very complex due to the presence of many magnetically unequivalent aromatic protons. In such cases, analyses of ESR spectra by computer simulation sometimes provide unequivocal hyperfine coupling (hfc) constants. To obtain the reliable proton hfc constants, ^{1}H ENDOR measurements were performed for **4** and **5** with toluene as the solvent at −65 °C. A typical ENDOR spectrum of **4** is drawn in Figure 4a. This spectrum was obtained by 25-times accumulation with a 111.94 kHz

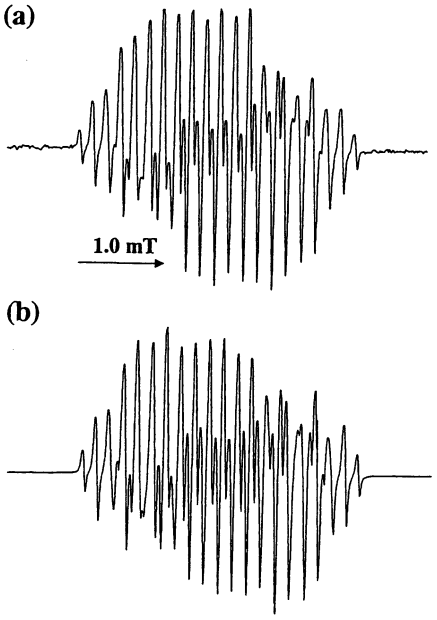

FIGURE 3. ESR spectrum of **4** in benzene measured at room temperature: (a) observed spectrum and (b) computer simulation. The hfc constant for *tert*-butyl protons was not input in the computer simulation.

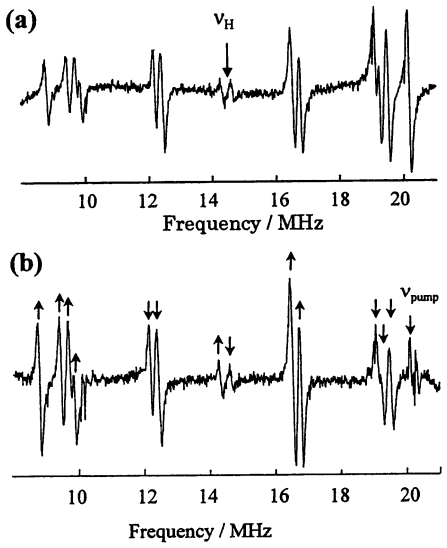

FIGURE 4. ^{1}H ENDOR and TRIPLE resonance spectra of **4** in toluene measured at −65 °C: (a) ENDOR spectrum and (b) TRIPLE resonance spectrum. In the TRIPLE resonance spectrum, the upward arrows (↑) indicate the increased peaks and the downward arrows (↓) indicate the decreased peaks.

modulation depth, showing 7 pairs of peaks. The innermost pair of peaks are assigned to the protons of *tert*-butyl groups, and the remaining 6 pairs of peaks are due to the protons of the pyrene ring. Since **4** has 7 pyrene ring protons, this result indicates that two pairs of peaks overlap into one pair of peaks. When the ENDOR spectra were measured with a lower modulation depth of 79.24 kHz, the pair of peaks with a hfc constant of 4.109 MHz split into two pairs of peaks with hfc constants of 4.065 and 4.125 MHz, though the S/N ratio was not good. Using the proton hfc constants determined by the ENDOR measurements, computer simulation of the ESR spec-

TABLE 1. Hyperfine Coupling Constants (mT) for 4, 4-d_4, and 5 Determined by ^{1}H ENDOR and ESR Spectroscopy

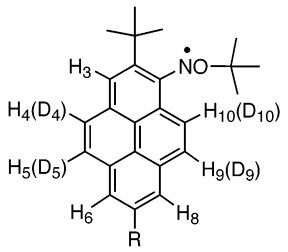

4: R = *t*-Bu, **5**: R = H_7

radical	method	solvent	temp/°C	a(N)[a]	a(H_3)	a(H_4 and H_{10})	a(H_5 and H_9)	a(H_6 and H_8)	a(H_7)	a(*t*-Bu)[b]	g
4	ENDOR	toluene	−65	0.672	0.164	0.147, 0.154	0.360, 0.407	0.331, 0.340		0.011	2.0035
4-d_4	ENDOR	mineral oil	27	0.672	0.167	0.023,[c] 0.023[c]	0.055,[d] 0.062[d]	0.331, 0.340		0.011	2.0035
5	ENDOR	toluene	−65	0.675	0.164	0.146, 0.152	0.363, 0.406	0.338, 0.340	0.105	0.011	2.0037

[a] Determined by computer simulation of the ESR spectra of the radicals in benzene measured at 20 °C. [b] The hfc constants for *tert*-butyl protons. The assingment of the *tert*-butyl group was not performed. [c] The hfc constants for D_4 and D_{10}. [d] The hfc constants for D_5 and D_9.

trum of **4** was carried out, varying the nitrogen hfc constant, and when a_N was 0.672 mT, an excellent agreement with the experimental spectrum was observed, as found in Figure 3.

When ENDOR spectra of **5** were measured with a modulation depth of 79.24 kHz, the spectrum obtained showed 9 pairs of peaks. The innermost pair of peaks are assigned to the protons of a *tert*-butyl group(s), and the remaining 8 pairs of peaks are due to the protons of the pyrene ring. Since **5** has 8 pyrene ring protons, detection of 8 pairs of peaks means that all pyrene ring protons could be observed. Using those proton hfc constants, the ESR spectrum of **5** was computer simulated, varying the nitrogen hfc constant, and when a_N was 0.675 mT, an excellent agreement with the experimental spectrum was obtained. The hfc constants for **4** and **5** determined by ESR and ENDOR are summarized in Table 1.

To determine the relative signs of the proton hfc constants experimentally, electron−nuclear−nuclear TRIPLE resonance measurements were performed.[11] The TRIPLE resonance spectrum of **4** is depicted in Figure 4b. When the peak at 20.16 MHz was pumped, the peaks at 12.18, 12.42, 14.63, 19.14, 19.27, and 19.53 MHz were decreased, and the peaks at 8.78, 9.42, 9.73, 9.86, 14.31, 16.53, and 16.79 MHz were increased. On the basis of the results of the above TRIPLE resonance it was concluded that the protons with the hfc constants of 0.407, 0.360, 0.340, and 0.331 mT have the same sign and the protons with the hfc constants of 0.164, 0.154, and 0.147 mT have the opposite sign.

The actual assignments of the protons are difficult without a partial deuteration of the pyrene ring protons. We therefore prepared a partially deuterated radical, **4**-d_4, starting from 2,7-di-*tert*-butyl-1-aminopyrene-*4,5,9,10*-d_4. The partially deuterated 2,7-di-*tert*-butyl-1-aminopyrene was previously prepared by our group.[10,12] The ENDOR measurements of **1**-d_4 were carried out at room temperature (27 °C) using mineral oil as the solvent. The observed ENDOR spectrum is shown in Figure 5, which shows 3 pairs of peaks. From the ENDOR spectrum, the proton with the hfc constant of 0.167 mT can be unequivocally assigned to H_3, and the protons with the hfc constants of 0.331 and 0.340 mT are assigned to H_6 and H_8. However, it is impossible to distinguish H_6 and H_8 at the present time.

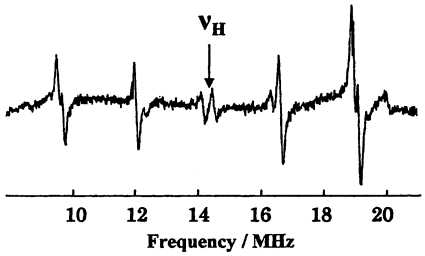

FIGURE 5. ^{1}H ENDOR spectrum of **4**-d_4 in mineral oil measured at 27 °C.

In the ESR spectrum of **4**-d_4 (Figure 6), small hyperfine couplings due to the deuteriums were observed. To accomplish an exact agreement between the observed and simulated spectra, the hfc constants due to the four deteriums were further added in computer simulation of **4**-d_4. The hfc constants for the deuteriums can be readily calculated using the equation $a_D = 0.1535a_H$. As found in Figure 6, an excellent agreement between the observed and simulated spectra is obtained by adding the hfc constants due to the deuteriums.

Assignments of two sets of H_4 and H_{10} and H_5 and H_9 were made on the basis of the relative signs of the protons determined by TRIPLE resonance spectroscopy. The ab initio molecular orbital calculations described below predict that H_5 and H_9 have the same sign as H_6 and H_8, while H_4 and H_{10} have the opposite sign for H_6 and H_8. This relation leads to the conclusion that H_4 and H_{10} are assigned to the protons with the hfc constants of 0.147 and 0.154 mT, and H_5 or H_9 are assigned to those with the hfc constants of 0.360 and 0.407 mT. However, more exact assignments to distinguish H_4 and H_{10} and H_5 and H_9 are impossible, similar to the case of H_6 and H_8.

(11) Biehl R.; Plato, M.; Moebius, K. *J. Chem. Phys.* **1975**, *63*, 3515. *Electron Nuclear Double Resonance Spectroscopy of Radical in Solution*; Kurreck, H., Kirste, B., Lubitz, W., Eds.; VCH Publishers: New York, 1988.

(12) Miura, Y.; Oka, H.; Yamano, E.; Morita, M. *J. Org. Chem.* **1997**, *62*, 1188−1190.

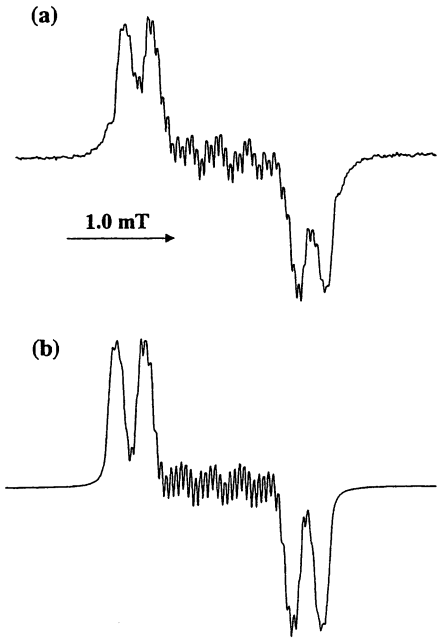

FIGURE 6. ESR spectrum of **4**-d_4 in benzene measured at room temperature: (a) observed spectrum and (b) computer simulation. The hfc constant for *tert*-butyl protons was not input in the computer simulation.

Ab Initio Molecular Orbital Calculations. Ab initio molecular orbital (MO) calculations based on the density functional theory were performed for **4** by the UBecke3LYP method using the STO 6-31G basis set. In the above calculations Gaussian 98W was used,[13] and the MO calculations are performed using the X-ray crystallographic structure. The total atomic spin densities are shown in Figure 7, and the calculated hfc constants are shown in Table 2. Although there is a rather large discrepancy between the calculated and observed a_N, the calculated proton hfc constants are in good agreement with the observed ones. Accordingly, the present MO calculations provide reliable results, revealing that the unpaired electron is extensively delocalized over the whole of the radical molecule.

Although it is important to determine the spin density on the oxygen for oxyaminyl radicals, the ESR method is incompetent because the natural abundance of ^{17}O isotope is very low (0.037%). One of the convenient and reliable methods is the MO calculations at a high quality level. The present MO calculations based on the density functional theory predict 0.096 for the spin density on the oxygen. This value is much lower than that of **1** (0.146). This is clearly explained by an extensive delocalization of the unpaired electron onto the pyrene ring.

(13) Frisch, M. J.; Trucks, G. W.; Schlegel, H. B.; Scuseria, G. E.; Robb, M. A.; Cheeseman, J. R.; Zakrzewski, V. G.; Montgomery, J. A., Jr.; Stratmann, R. E.; Burant, J. C.; Dapprich, S.; Millam, J. M.; Daniels, A. D.; Kudin, K. N.; Strain, M. C.; Farkas, O.; Tomasi, J.; Barone, V.; Cossi, M.; Cammi, R.; Mennucci, B.; Pomelli, C.; Adamo, C.; Clifford, S.; Ochterski, J.; Petersson, G. A.; Ayala, P. Y.; Cui, Q.; Morokuma, K.; Malick, D. K.; Rabuck, A. D.; Raghavachari, K.; Foresman, J. B.; Cioslowski, J.; Ortiz, J. V.; Baboul, A. G.; Stefanov, B. B.; Liu, G.; Liashenko, A.; Piskorz, P.; Komaromi, I.; Gomperts, R.; Martin, R. L.; Fox, D. J.; Keith, T.; Al-Laham, M. A.; Peng, C. Y.; Nanayakkara, A.; Challacombe, M.; Gill, P. M. W.; Johnson, B.; Chen, W.; Wong, M. W.; Andres, J. L.; Gonzalez, C.; Head-Gordon, M.; Replogle, E. S.; Pople, J. A. *Gaussian 98*, Revision A.9; Gaussian, Inc.: Pittsburgh, PA, 1998.

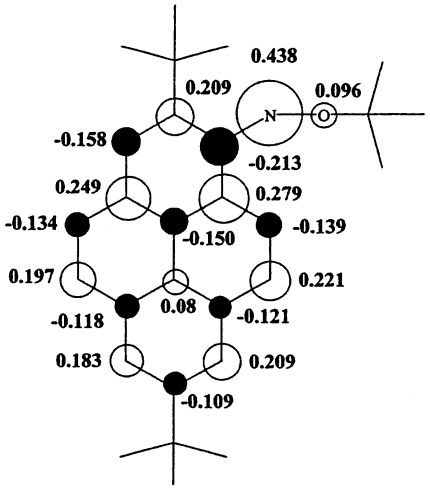

FIGURE 7. The total atomic spin densities in **4** calculated by the DFT UBecke 3LYP method using the STO 6-31G basis set.

TABLE 2. Comparison of the Experimental and Calculated Hfc Constants for 4

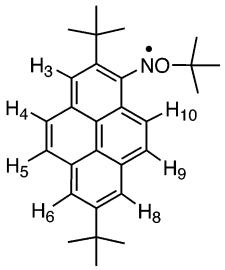

positionn	calcd hfc const[a,b]	obsd hfc const[a,c]
N	1.0644	0.672
O	−0.7601	
H_3	0.2930	0.164
H_4	0.2381	0.147 or 0.154
H_5	−0.4372	0.360 or 0.407
H_6	−0.4067	0.331 or 0.340
H_8	−0.4624	0.340 or 0.331
H_9	−0.5039	0.407 or 0.360
H_{10}	0.2604	0.154 or 0.147

[a] The hfc constants are expressed in mT. [b] The MO calculations are performed at the DFT UBecke 3LYP/STO 6-31G level. [c] The observed hfc constants are shown as absolute values.

Magnetic Susceptibility Measurements. The magnetic properties of the isolated butoxyaminyl radicals **4** and **5** were measured with a SQUID magnetometer using polycrystalline samples in the temperature range 1.8−300 K. The diamagnetic contributions were estimated using Pascal's constants. The radical samples were twice recrystallized from MeOH (**4**) or MeOH-EtOAc (**5**). The purities of **4** and **5** determined by ESR were 93 and 95%, respectively.

The χ_{mol} vs T plots for **4** are depicted in Figure 8. The purity of **4** determined by SQUID was 90%, which was somewhat lower than that determined by ESR. The χ_{mol} value increases with decreasing temperature and gives a maximum at 10 K. Below 10 K, the χ_{mol} value decreases a little and again increases. This increase is due to the presence of the defects in the crystals. The χ_{mol} vs T plots were analyzed with the alternating linear chain model

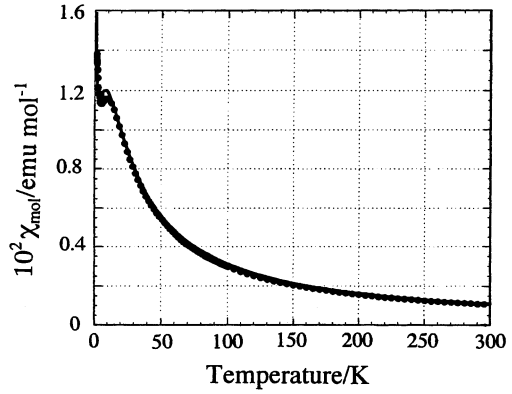

FIGURE 8. The χ_{mol} vs T plots for **4**. The solid line indicates the values calculated by the modified alternating linear chain model (eq 1) with $2J/k_B = -20$ K, $\alpha = 0.83$, and $x = 0.06$.

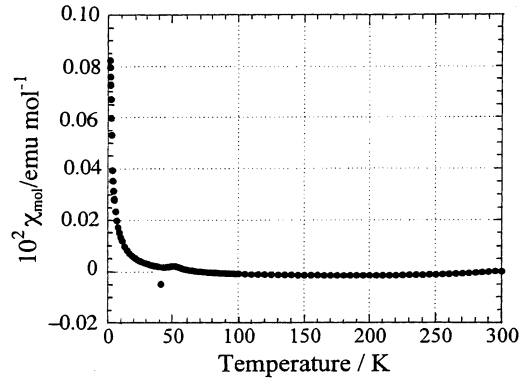

FIGURE 9. The χ_{mol} vs T plots for **5**.

described by eq 1. In eq 1, the presence of the Curie paramagnetic components is taken into account. The best fit of the theoretical curve with the experimental results gave $2J/k_B = -20$ K, $\alpha = 0.83$, and $x = 0.06$.

$$H = -(0.90 - x)2J\sum(S_{2i-1}\cdot S_{2i} + \alpha S_{2i}\cdot S_{2i+1}) + xC/T \quad (1)$$

Radical **5** showed an unusually strong antiferromagnetic interaction. As found in Figure 9, the χ_{mol} value was already $\approx$0 emu mol^{-1} at 300 K, indicating that the absolute value of the antiferromagnetic interaction, $|2J/k_B|$, is much larger than 300 K.

The magnetic behavior of **4** and **5** was explained by their crystal structures. In Figure 10, the crystal structure of **4** is depicted. The shortest distance between the neighboring radical molecules is found for C8- - -C12′, whose distance is 4.05 Å. The second shortest distance of 4.26 Å is found for C6- - -C10′. According to the McConnell mechanism, the relative signs of the spin densities on those atoms are opposite each other.[14] This leads to the intermolecular antiferromagnetic interaction between the neighboring radical molecules, which agrees with the observed antiferromagnetic results. However, there is a discrepancy between the magnetic behavior and the X-ray results. Although Figure 10 shows that **4** has a uniform chain structure at room temperature, the magnetic behavior is better described by the alternating

(14) McConnell, H. M. *J. Chem. Phys.* **1963**, *39*, 1910.

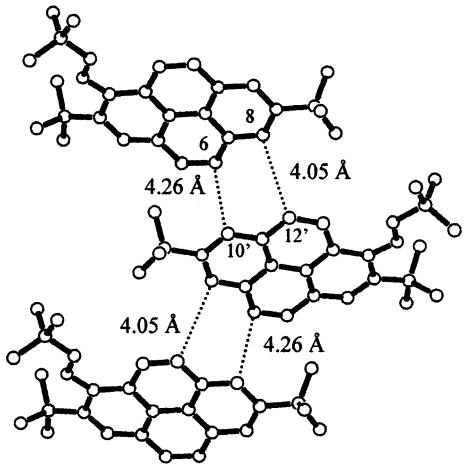

FIGURE 10. The crystal structure of **4**.

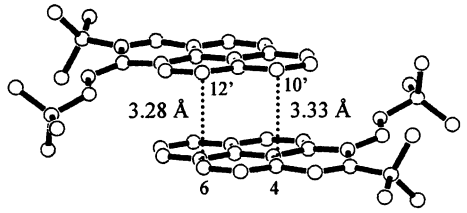

FIGURE 11. The crystal structure of **5**.

model. For this discrepancy, a plausible explanation is the breaking of the uniform chain structure of the crystal at low temperatures. Another possible explanation may be the presence of the diamagnetic (10%) components, which break intermolecular interaction.

Figure 11 shows that **5** forms a dimer in which the two radical molecules face in an antisymmetric fashion. The shortest intermolecular distance within the dimer is found for C6- - -C12′, whose distance is 3.28 Å. On the other hand, the shortest distance between the dimers is more than 6.0 Å, which is too long for interaction. According to the McConnell mechanism, the intermolecular interaction within the dimer should be antiferromagnetic. Since the spin densities on C6 and C12′ are very high and the two radicals contact through the short distance between C6 and C12′, the observed very strong antiferromagnetic interaction can be well explained by its crystal structure.

Conclusions

In this study two kinds of pyrene ring bearing *N-tert*-butoxyaminyls, **4** and **5**, were isolated as radical crystals. The nitrogen and proton hyperfine coupling constants were unequivocally determined by measuring the ESR and ^{1}H ENDOR/TRIPLE resonance spectra. The pyrene ring proton hyperfine coupling constants were assigned with the aid of a partially deuterated radical. The X-ray crystallographic analyses were performed for **4** and **5**, showing that both radicals adopt a planar conformation. The magnetic susceptibility measurements were performed for the isolated radicals. Radical **4** showed a weak antiferromagnetic interaction, and the antiferromagnetic behavior was analyzed with the alternating linear chain model, giving $2J/k_B = -20$ K and $\alpha = 0.83$. On the other

hand, **5** showed a strong antiferromagnetic interaction ($|2J/k_B| > 300$ K). The magnetic interactions observed for **4** and **5** were well explained by their crystal structures.

Experimental Section

General. IR, UV−vis, ^{1}H NMR, and ESR spectra were recorded as previously reported.[15] ^{1}H ENDOR measurements were carried out on a Bruker 300/350 ENDOR spectrometer equipped with a TM_{011} mode microwave cavity operating at X-band. Magnetic susceptibility measurements were performed with a Quantum Design MPMS2 magnetometer using polycrystalline samples in the temperature range 1.8−300 K. The diamagnetic components were estimated by Pascal's sum rule.

Materials. 2-*tert*-Butyl-1-aminopyrene,[9] 7-*tert*-butyl-1-aminopyrene,[8] 2,7-di-*tert*-butyl-1-aminopyrene,[8] and 2,7-di-*tert*-butyl-1-aminopyrene-*4,5,9,10*-d_4[10] (*d* content 87%) were prepared by our previously reported methods. *tert*-Butyl peroxybenzoate (Aldrich) was commercially available and used without purification. Alumina column chromatography was performed on Merck aluminum oxide 90.

***N*-*tert*-Butoxy-2,7-di-*tert*-butyl-1-pyrenylaminyl (4).** A solution of 0.880 g (2.67 mmol) of 2,7-di-*tert*-butyl-1-aminopyrene in 50 mL of anhyd THF was cooled to −78 °C under N_2, and 1.9 mL (2.9 mmol) of a butyllithium hexane solution (1.55 M) was added with a syringe. After being stirred for 10 min at the same temperature, a solution of 1.71 g (8.80 mmol) of *tert*-butyl peroxybenzoate in 10 mL of anhyd THF was added with a syringe. After being stirred for 1.5 h at the same temperature, the mixture was raised to ∼0 °C and water was added. The reaction mixture was extracted with benzene, and the benzene layer was washed with brine and dried over anhyd $MgSO_4$. After filtration, the filtrate was evaporated under reduced pressure, and the residue was column chromatographed on alumina with 1:4 benzene−hexane. Recrystallization from MeOH gave dark red plates with mp 129−130 °C in 27% yield (0.288 g, 0.720 mmol). UV−vis (]benzene) λ (ϵ) 301 (8430), 357 (12300), 406 (25000), 428 nm (29300 L mol^{-1} cm^{-1}). Anal. Calcd for $C_{28}H_{34}NO$: C, 83.95; H, 8.56; N, 3.50. Found: C, 83.99; H, 8.58; N, 3.54.

***N*-*tert*-Butoxy-2,7-di-*tert*-butyl-1-pyrenylaminyl-4,5,9,-10-d_4 (4-d_4).** In the same procedure as for **4**, this partly deuterated pyrenylaminyl radical was prepared from 2,7-di-*tert*-butyl-1-aminopyrene-*4,5,9,10*-d_4. Recrystallization from MeOH gave dark green plates with mp 126−128 °C in 15% yield. Anal. Calcd for $C_{28}H_{30}D_4NO$: C, 83.12; H, 7.47; N, 3.46. Found: C, 83.01; H, 7.23; N, 3.52.

***N*-*tert*-Butoxy-2-*tert*-butyl-1-pyrenylaminyl (5).** A solution of 0.730 g (2.67 mmol) of 2-*tert*-butyl-1-aminopyrene in 50 mL of anhyd THF was cooled to −78 °C under N_2, and 1.9 mL (2.9 mmol) of a butyllithium hexane solution (1.55 M) was added with a syringe. After the mixture was stirred for 10 min at the same temperature, a solution of 1.71 g (8.80 mmol) of *tert*-butyl peroxybenzoate in 10 mL of anhyd THF was added with a syringe. After being stirred for 1.5 h at the same temperature, the mixture was raised to ∼0 °C and water was added. The reaction mixture was extracted with benzene, and the benzene extract was washed with brine and dried over anhyd $MgSO_4$. After filtration, the filtrate was evaporated under reduced pressure, and the residue was column chromatographed on alumina with 1:4 benzene−hexane. Recrystallization from MeOH-EtOAc gave dark green plates with mp 163−164 °C in 23% yield (0.213 g, 0.618 mmol). UV−vis (benzene) λ (ϵ) 300 (7670), 357 (12000), 403 (22100), 422 nm (25800 L mol^{-1} cm^{-1}). Anal. Calcd for $C_{24}H_{26}NO$: C, 83.68; H, 7.61; N, 4.07. Found: C, 83.77; H, 7.74; N, 3.92.

X-ray Crystallographic Analyses. All measurements were made on a Rigaku AFC7R diffractometer with graphite monochromated MoKα radiation (λ = 0.71069 Å) at 23 ± 1 °C.

4: a dark platelet crystal of $C_{28}H_{34}NO$ having approximate dimensions of 0.60 × 0.60 × 0.10 mm^3; orthorhombic space group P_{bca} (no. 61), a = 37.676(7) Å, b = 11.766(4) Å, c = 10.851(6) Å, V = 4809(6) Å^3, D = 1.106 g cm^{-3}. Of the 15505 reflections measured 7039 were unique (R_{int} = 0.059), 2987 of which were considered as observed ($I > 1.50\sigma(I)$). The structure was solved by direct methods (SIR92)[16] and expanded using Fourier techniques.[17] The non-hydrogen atoms were refined anisotropically, and all hydrogen atoms were placed at the calculated positions and not refined. The final cycle of full-matrix least-squares refinement was based on 2987 observed reflections and 299 variable parameters and converged with unweighted and weighted agreement factors of R = 0.075[18] and R_w = 0.134.[19] GOF = 1.33.[20]

5: a green platelet crystal of $C_{24}H_{26}NO$ (344.48) having approximate dimensions of 0.50 × 0.40 × 0.20 mm^3; monoclinic space group $P2_1/c$ (no.14), a = 16.0862(7) Å, b = 9.9106(3) Å, c = 12.1183(5) Å, β = 90.891(4)°, V = 1931.7(1) Å^3, Z = 4, D_c = 1.184 g cm^{-3}. Of the 16827 reflections measured 4211 were unique (R_{int} = 0.042), 2872 of which were considered as observed ($I > 3.00\sigma(I)$). The structure was solved by direct methods (SIR92)[16] and expanded using Fourier techniques.[17] The non-hydrogen atoms were refined anisotropically. Hydrogen atoms were placed in the fixed position and not refined. The final cycle of full-matrix least-squares refinement was based on 2872 observed reflections and 339 variable parameters and converged with unweighted and weighted agreement factors of R = 0.085[18] and R_w = 0.131.[19] GOF = 1.90.[20]

Supporting Information Available: X-ray crystallographic data; tables of atomic coordinates, thermal parameters, bond lengths, bond angles, and torsion angles for **4** and **5**. This material is available free of charge via the Internet at http://pubs.acs.org.

JO0202785

(15) Miura, Y.; Momoki, M.; Nakatsuji, M.; Teki, Y. *J. Org. Chem.* **1998**, *63*, 1555−1565.

(16) Altomare, A.; Burla, M. C.; Camalli, M.; Cascarano, M.; Giacovazzo, C.; Guagliardi, A.; Polidori, G. *J. Appl. Crystallogr.* **1994**, *27*, 435.

(17) DIRDIF94: Beurskens, P. T.; Admiraal, G.; Beurskens, G.; Bosman, W. P.; de Gelder, R.; Israel, R.; Smits, J. M. M. Technical Report of the Crystallography Laboratory, University of Nijmegen, The Netherlands, 1994.

(18) $R = \sum(F_o^2 - F_c^2)/\sum F_o^2$.

(19) $R_w = [\sum w(F_o^2 - F_c^2)^2/\sum w(F_o^2)^2]^{1/2}$.

(20) The crystallographic computing was done by the TEXANE structure analysis software.